Orthogonality catastrophe and decoherence in a trapped-Fermion environment

A. Sindona[1,2], J. Goold[3,4], N. Lo Gullo[3,5], S. Lorenzo[1,2], F. Plastina[1,2]
[1]*Dipartimento di Fisica, Università della Calabria, 87036 Arcavacata di Rende (CS), Italy*
[2]*INFN sezione LNF-Gruppo collegato di Cosenza, Italy*
[3]*Clarendon Laboratory, University of Oxford, United Kingdom*
[4]*Physics Department,University College Cork, Cork, Ireland*
[5]*Quantum Systems Unit, Okinawa Institute of Science and Technology and Graduate University, Okinawa, Japan*
(Dated: November 8, 2012)

The Fermi edge singularity and the Anderson orthogonality catastrophe describe the universal physics which occurs when a localized scattering potential is suddenly introduced in a Fermi sea leading to a brutal disturbance of the ground state. We demonstrate that the effect can be seen in the controllable domain of ultracold trapped gases by providing an analytic description the out-of-equilibrium response to an atomic impurity, both at zero and at finite temperature. Furthermore, we link the transient behavior of the gas to the decoherence of the impurity, and, in particular to the amount of non-markovianity present in its dynamics.

PACS numbers: 67.85.-d, 05.30.Fk, 03.65.Yz

A Fermi gas may be shaken-up by the switching of even a single, weakly interacting impurity, producing a complete rearrangement of the many body wave-function that, as a consequence, loses essentially any overlap with the initial, unperturbed one. This is the essence of Anderson's orthogonality catastrophe [1], witnessed by the singular (edge-like) behavior of the energy distribution of the impurity induced excitations. An example of how such a many-body effect comes into play is provided by X-ray photoemission spectra from most simple metals [2, 3], where the expected sharp symmetric peak at the binding energy of a core level is converted into a power law singularity. Similar patterns have been observed in electron emission via X-ray absorption and Auger neutralization from carbon based nanomaterials [4], and recently predicted for quantum dots [5]. Fermi edge resonance and orthogonality catastrophe have been also revealed by non-equilibrium current fluctuations (shot noise) in nano-scale conductors [6], and enter prominently the physics of phenomena as diverse as the Kondo effect [7] and the scattering or sticking of a low-energy atom or ion on a metal surface [8, 9].

Recently, it has been proposed to observe this universal physics in controllable ultracold atomic setups where the singular behavior may be probed either in the time domain by Ramsey interference type experiments, performed on the impurity atom [10], or in the frequency domain by radio-frequency spectroscopy [11]. However, an analytic framework for the case of a *trapped* Fermi gas is lacking. In this letter we provide such an analytic description, and discuss the transient response of a harmonically trapped Fermi gas following the '*sudden*' switching of an embedded two-level atom excited by a fast pulse. The switching of the *local* impurity produces a local quench of the gas, giving rise to the Anderson catastrophe. We propose a study of the Fermi-edge physics at zero and finite temperature and both in the frequency domain, by looking at the excitation spectrum of the gas, and in the time domain, by studying the decoherence dynamics of the impurity. This allows us to link the Fermi edge behavior of the excitation energy distribution to the dynamics of the impurity, and, in particular, to the Loschmidt echo [12, 13]. Furthermore, we investigate the non-Markovianity of the induced dynamics using recently developed tools [14–17], which have been employed to study open systems in different environments, ranging from spins [18] to Bose-Einstein condensates [19], and experimentally tested in optical set-ups [20, 21]. We find that the non-Markovianity of the decoherent dynamics provides a novel interpretation of the essential physics of the process. Specifically, we consider a gas of non-interacting cold fermions confined by a one-dimensional trapping harmonic potential of frequency ω, described by the Hamiltonian $\hat{H}_0 = \sum_n \varepsilon_n \hat{C}_n^\dagger \hat{C}_n$, with C_n being the annihilation operator for the n-th single particle level of energy $\varepsilon_n = \hbar\omega(n + 1/2)$. An impurity is present in the gas, constituted by a two-level atom with energy separation $\hbar\Omega$, localized at the minimum of the potential well. The fermions lie in their equilibrium configuration, set by $\hat{H}_0$, until the impurity is excited and a sudden perturbation $\hat{V}(t) = \hat{V}\theta(t)$ is felt by the gas. To mimic a very strong difference in scattering length depending on the internal state of the impurity, we model it by a spatially localized (delta-like) potential, activated by the population of the excited state, $\hat{V} = V(x) \otimes |e\rangle\langle e|$, where $V(x) = \pi V_0 x_0 \delta(x)$. Here, V_0 is the coupling constant and x_0 is the characteristic length of the harmonic potential. Only even one-fermion states (with $n = 2r$) are involved in the shake-up process, being coupled by the matrix elements $V_{rr'} = V_0 (-1)^{r+r'} {}_2\Gamma_1(r)^{1/2} {}_2\Gamma_1(r')^{1/2}$, with ${}_2\Gamma_1$ denoting the Euler's gamma-function ratio ${}_2\Gamma_1(r) = \Gamma(r + 1/2)/\Gamma(r+1)$. Without loss of generality, we may assume the Fermi number to be even so that the Fermi energy reads $\varepsilon_{\rm F} = \hbar\omega(2r_{\rm F} + 1/2)$, with level occupation numbers given by the Fermi factors $f_r = \left(1 + e^{2\beta\hbar\omega r}\right)^{-1}$.

A key quantity for the following is the so-called *vacuum persistence amplitude*

$$\nu_\beta(t > 0) = \left\langle e^{\frac{i}{\hbar}\hat{H}_0 t} e^{-\frac{i}{\hbar}(\hat{H}_0+\hat{V})t} \right\rangle, \qquad (1)$$

with $\langle \ldots \rangle$ denoting the thermal equilibrium average over the unperturbed environment states. ν_β is the probability amplitude that the environment will retrieve its equilibrium state at time t, after the switching on of the perturbation and, as dis-

cussed below, it gives the decoherence factor for the impurity. The Fourier transform

$$\tilde{\nu}_\beta(E) = \int_{-\infty}^{\infty} \frac{dt}{2\pi\hbar}\, e^{\frac{itE}{\hbar}}\, \nu_\beta(t), \tag{2}$$

subject to the analytical constraint $\nu_\beta(t<0) = \nu_\beta^*(-t)$, is the excitation spectrum relative to the unperturbed energy.

In the interaction picture we get

$$\nu_\beta(t) = \left\langle T e^{-\frac{i}{\hbar}\int_0^t dt' \tilde{V}(t')} \right\rangle, \quad \tilde{V}(t) = e^{\frac{i}{\hbar}\hat{H}_0 t} \hat{V} e^{-\frac{i}{\hbar}\hat{H}_0 t}, \tag{3}$$

which, by virtue of the linked cluster theorem, reduces to an exponential sum of connected Feynmann diagrams, $\nu_\beta(t) = \exp\{\Lambda_\beta(t)\}$, with:

$\Lambda_\beta(t) =$ 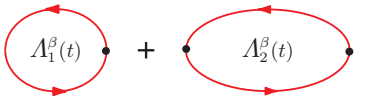 $+ \cdots$

After introducing the unperturbed propagator

$$i\hbar G_r^\beta(t) = e^{-i(2r+1/2)\omega t}\left[\theta(t)\, f_{r_\mathrm{F}-r} - \theta(-t)\, f_{r-r_\mathrm{F}}\right], \tag{4}$$

and applying Wick's theorem, we focus on the loops with one and two vertices, namely, $\Lambda_1^\beta(t)$ and $\Lambda_2^\beta(t)$. These diagrams contain separable products of arrows (G_r^β) connected to vertices ($V_{rr'}$). In terms of the auxiliary functions

$$\lambda_\pm^\beta(t) = \sum_r {}_2\Gamma_1(r)\; e^{\pm 2ir\omega t} f_{\pm(r-r_\mathrm{F})}, \tag{5}$$

we may express the diagrams as

$$\Lambda_1^\beta(t) = -\frac{it}{\hbar}\sigma V_0 \lambda_+(0), \tag{6}$$

$$\Lambda_2^\beta(t) = -\frac{\sigma V_0^2}{\hbar^2}\int_0^t dt' \int_0^{t'} dt''\, \lambda_+^\beta(t'')\; \lambda_-^\beta(-t''). \tag{7}$$

We will see in the following that the relevant energy scale for the problem is set by $\sqrt{\hbar\omega\varepsilon_\mathrm{F}}$, involving both the level separation and the Fermi energy. Therefore, we introduce $\alpha = \frac{\sigma V_0^2}{2\,\hbar\omega\,\varepsilon_\mathrm{F}}$ as a sensible parameter, ranging typically from 0 to 1 (σ accounts for the spin degeneracy). The contribution (6) is then written as $\Lambda_1^\beta(t) = -itE_1^\beta/\hbar$, where

$$E_1^\beta = \sqrt{2\sigma\hbar\omega\varepsilon_\mathrm{F}\alpha}\sum_{r=0}^{r_\mathrm{F}} {}_2\Gamma_1(r)\; f_{r-r_\mathrm{F}}, \tag{8}$$

is nothing but the first-order correction, as obtained by using Rayleigh-Schrödinger perturbation theory, to the unperturbed energy $E_0^\beta = \sum_n \varepsilon_n\, f_{n/2-r_\mathrm{F}}$, which is plotted in Fig. 1**A**. Then, $\Lambda_1^\beta(t)$ brings a phase factor to $\nu_\beta(t)$, which corresponds to shifting the spectrum $\tilde{\nu}_\beta(E)$ by E_1^β, whose behavior vs ε_F is shown in Fig. 1**B**. We notice that E_0^β is 1 to 3 orders of magnitude larger than E_1^β, depending on β and ε_F, while temperature plays an appreciable role in both E_0^β and E_1^β for $\varepsilon_\mathrm{F}/\hbar\omega$ below ~ 100, and $\beta\hbar\omega$ less than ~ 0.1.

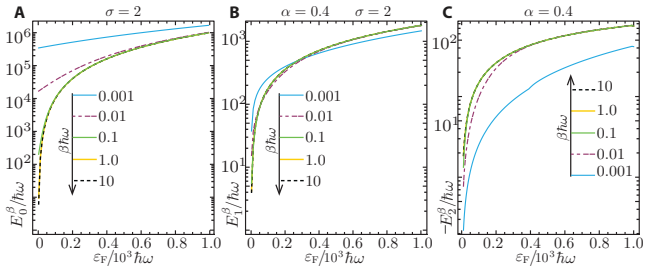

FIG. 1. (Color online) Unperturbed equilibrium energy E_β^0 of a spin-1/2 gas into a harmonic trap (panel **A**), and perturbation corrections E_β^1 (panel **B**), E_β^2 (panel **C**), due to the sudden switching potential $V(x)$. Energies are reported in units of $\hbar\omega$ *vs* $\varepsilon_\mathrm{F}/\hbar\omega$ for values of $\beta\hbar\omega$ in the range of 0.001 to 1, and in the $\beta\hbar\omega \to \infty$ limit (absolute zero). Finite temperature summations are computed from Eqs. (8) and (12), with $\alpha = 0.4$, using a high energy cut-off $r < 10^2 r_\mathrm{F}$.

Performing the time-ordered integrals in (7), we rewrite the two-vertex connected graph as

$$\Lambda_2^\beta(t) = -\frac{\alpha\varepsilon_\mathrm{F}}{\hbar}\sum_{r,r'=0}^{\infty}\left[it\varphi_{rr'} - \frac{\psi_{rr'}(t)}{2\omega}\right] f_{r-r_\mathrm{F}} f_{r_\mathrm{F}-r'}, \tag{9}$$

in which

$$\varphi_{rr'} = \frac{{}_2\Gamma_1(r)\; {}_2\Gamma_1(r')}{r-r'}, \tag{10}$$

$$\psi_{rr'}(t) = {}_2\Gamma_1(r)\; {}_2\Gamma_1(r')\; \frac{1-e^{2i(r-r')t\omega}}{(r-r')^2}. \tag{11}$$

Here, we may separate the sums over even-state labels (r,r') into three contributions with well defined trends, $\Lambda_2^\beta(t) = \Lambda_{2\mathrm{S}}^\beta(t) + \Lambda_{2\mathrm{G}}^\beta(t) + \Lambda_{2\mathrm{P}}^\beta(t)$, where the subscript stand for Shift, Gaussian and Periodic, respectively. In particular, the off-diagonal summands in (9) that multiply $\varphi_{rr'}$ provide a (further) shift to the environment energy, the second-order correction $\Lambda_{2\mathrm{S}}^\beta(t) = -itE_2^\beta/\hbar$, with

$$E_2^\beta = -\varepsilon_\mathrm{F}\alpha \sum_{\substack{r,r'=0 \\ r\neq r'}}^{\infty} \varphi_{rr'} f_{r-r_\mathrm{F}} f_{r_\mathrm{F}-r'}. \tag{12}$$

In Fig. 1**C**, we notice that E_2^β takes absolute values similar to E_1^β, but it is more sensitive to temperature, for $\beta\hbar\omega < 0.05$. The diagonal elements of Eq. (9) yield a quadratic power law

$$\Lambda_{2\mathrm{G}}^\beta(t) = -\alpha\omega\frac{\varepsilon_\mathrm{F}}{\hbar}t^2 g_\beta, \tag{13}$$

which produces a gaussian damping in $\nu_\beta(t)$, and a gaussian broadening in $\tilde{\nu}_\beta(E)$, depending on the coefficient

$$g_\beta = \sum_{r=0}^{\infty} {}_2\Gamma_1(r)^2\; f_{r-r_\mathrm{F}} f_{r_\mathrm{F}-r}. \tag{14}$$

The broadening parameter is weakly influenced by the

Fermi energy, but strongly affected by temperature, inducing changes of various orders of magnitudes for $\beta\hbar\omega < 2$ and tending to $\alpha\omega^2$ in the zero temperature limit (Fig.2**A**).

The most important content of the second diagram $\Lambda_2^\beta(t)$, giving a non trivial structure to $\nu_\beta(t)$, arises from the series

$$\Lambda_{2\mathrm{P}}^\beta(t) = -\frac{\varepsilon_\mathrm{F}\alpha}{2\hbar\omega}\sum_{\substack{r,r'=0\\ r\neq r'}}^{\infty}\psi_{rr'}(t)\, f_{r-r_\mathrm{F}}\, f_{r_\mathrm{F}-r'} \qquad (15)$$

being periodic in time with frequency ω (see Fig. 2**B**). The zeroes of this sub-graph, when combined with the gaussian damping (13), yield modulations in the vacuum persistence amplitude which, as discussed below, are a signature of non-markovianity.

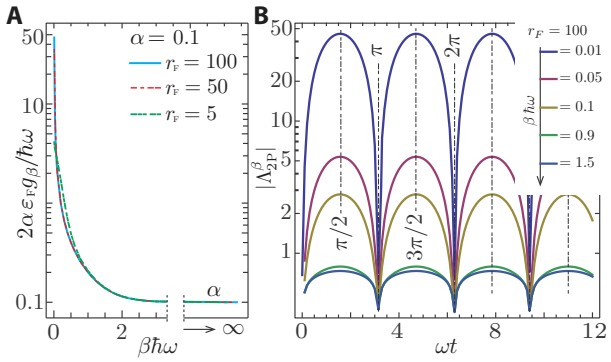

FIG. 2. (color online): (**A**) Gaussian broadening of eq. (13) in ω^2-units *vs* $\beta\hbar\omega$ for $r_\mathrm{F} = 5, 50, 100$, and $\alpha = 0.1$. (**B**) Modulus of the sub-diagram $\Lambda_{2\mathrm{E}}^\beta(t)$ (15), displaying periodic behavior with respect to ωt, represented for $\beta\hbar\omega = 0.01 - 1.5$, $r_\mathrm{F} = 100$, and $\alpha = 0.1$.

The Gaussian power law of Eq. (13) and the periodic contribution of Eq. (15) can be approximated as [22]

$$\Lambda_{2\mathrm{G}}^\beta(t) \approx -\frac{\alpha\omega^2 t^2}{2}\left[1 + 8\sum_{m=1}^{\infty}\frac{(-1)^m m}{e^{2m\beta}-1}\right]. \qquad (16)$$

$$\begin{aligned}\Lambda_{2\mathrm{P}}^\beta(t) = {} & \ln\left(\frac{e^{2\tau_0\omega}-1}{e^{2\omega(\tau_0+it)}-1}\right)^\alpha \\ & + \sum_{m=0}^{\infty}\ln\left[\frac{1-e^{-2(m+1)\beta\hbar\omega}}{1-e^{2(it-(m+1)\beta\hbar)\omega}}\right]^\alpha \\ & + \sum_{m=1}^{\infty}\ln\left[\frac{e^{2m\beta\hbar\omega}-1}{e^{2(it+m\beta\hbar)\omega}-1}\right]^\alpha, \end{aligned} \qquad (17)$$

where τ_0 is a regularization parameter (needed since $\Lambda_{2\mathrm{P}}^\beta(t)$ is singular at $\tau_0 \to 0^+$), that we can interpret as the typical time-scale over which environment transitions occur. Notice that thermal fluctuations introduce other characteristic times $\tau_m = m\beta\hbar$.

Numerical calculations of $\nu_\beta(t)$ at Fermi numbers below $r_\mathrm{F} = 100$ may be run straightforwardly, using Eqs. (13) and (15), but an analytic approximation is easily obtained as well: leaving aside the shifts due to Eqs. (8) and (12), the non trivial part of the vacuum persistence amplitude is

$$\nu'_\beta(t) = e^{-\alpha\omega\varepsilon_\mathrm{F} g_\beta t^2/\hbar} e^{\Lambda_{2\mathrm{P}}^\beta(t)}. \qquad (18)$$

Of particular interest is the behavior of $|\nu_\beta(t)|$ exhibiting spikes at $\omega t \sim \pi, 2\pi, \ldots$, which become more and more pronounced with increasing $\beta\hbar\omega$, see left panels in Fig. 3.

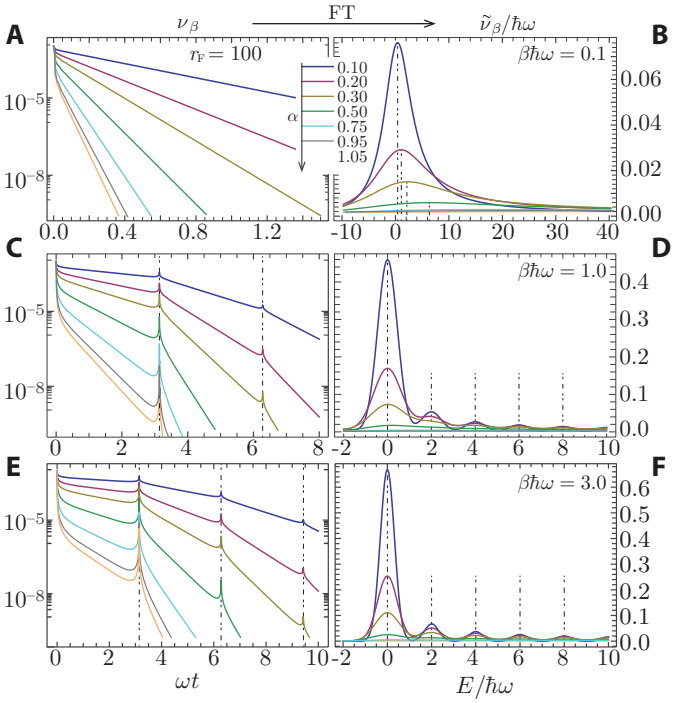

FIG. 3. (color online): Absolute value of the decoherence factor $|\nu_\beta(t)|$ (left panels, **A**,**C**,**E**) and absorption spectrum $\nu'_\beta(E)$ (right panels, **B**,**D**,**F**), calculated from eq. (18) by numerically computing the sub-diagrams of eqs. (13) and (15), for $\beta\hbar\omega = 0.1 - 10$, $r_\mathrm{F} = 100$, and $\alpha = 0.1 - 1.05$.

The periodicity in the time domain is reflected in the absorption spectrum $\tilde{\nu}_\beta(E)$ that offers an asymmetric, broadened, signature of the singular behavior of the fermion environment. The monotonic structure turns into a sequence of sub-peaks, separated by $2\hbar\omega$ and related to even-level transitions in the gas as $\beta\hbar\omega$ gets above ~ 0.5 (see Fig. 3**B**). These features are observed for any r_F in the range of 5 to 100 [22]. Eqs. (16) and (17) give the following form to the vacuum persistence amplitude at zero temperature,

$$\nu'_\infty(t) \approx e^{-\alpha t^2\omega^2/2}\left(\frac{e^{2\tau_0\omega}-1}{e^{2\omega(\tau_0+it)}-1}\right)^\alpha, \qquad (19)$$

which we checked to accurately reproduce the exact numerical result for Fermi numbers larger than 10, for suitable values of the cut-off parameter, say, $\tau_0\omega \sim 0.01$ (see Fig. 4**A**).

We now compare our results to the one-dimensional free-fermion case. To this end, we keep α and ε_F constant, letting $\hbar\omega \to 0$ with $2r_\mathrm{F} \approx \varepsilon_\mathrm{F}/\hbar\omega$ being large but not infinite. No

gaussian damping occurs in this case, while $\Lambda_{2\mathrm{P}}^{\infty}(t)$ tends to

$$\Lambda_{\mathrm{MND}}(t) = \log\left(\frac{1}{it/\tau_0+1}\right)^{\alpha}, \tag{20}$$

yielding the Mahan-Nozieres-De Dominicis (MND) propagator $\nu_{\mathrm{MND}}(t) = (it/\tau_0+1)^{-\alpha}$, originally calculated for a suddenly switched core-hole in a free electron gas [2, 3]. The parameter $\hbar/\tau_0$ coincides with the effective energy range of the core-hole potential around the Fermi energy, and α is the MND critical parameter. Interestingly, in our case the α-parameter bears the same range of criticality as the MND parameter ($\alpha = 0-1$). Finally we notice that temperature effects are mainly contained in

$$\nu'_{\beta}(t) \approx e^{-\frac{\alpha\omega^2t^2}{2}\left[1+8\sum_{m=1}^{\infty}\frac{(-1)^m m}{e^{2m\beta}-1}\right]}\left(\frac{e^{2\tau_0\omega}-1}{e^{2\omega(\tau_0+it)}-1}\right)^{\alpha}$$
$$\prod_{m=0}^{\infty}\left(\frac{1-e^{-2(m+1)\beta\hbar\omega}}{1-e^{2(it-(m+1)\beta\hbar)\omega}}\right)^{\alpha}\left(\frac{e^{2m\beta\hbar\omega}-1}{e^{2(it+m\beta\hbar)\omega}-1}\right)^{\alpha}$$

which provides an excellent approximation of Eq. (19).

Up to now, we treated the response of the Fermi gas without any reference to the dynamics of the impurity, that has just been assumed in the excited states for $t \geq 0$. If, instead, the two-level atom is subject to (say) a $\pi/2$ pulse and prepared in the superposition $(|g\rangle + |e\rangle)/\sqrt{2}$, it experiences a purely dephasing dynamics such that its state at later times is $\rho_{\mathrm{IMP}}(t) = (|g\rangle\langle g| + |e\rangle\langle e| + \nu_{\beta}(t)|g\rangle\langle e| + \mathrm{h.c.})/2$. The decoherence factor that enters the off-diagonal elements is just the persistence amplitude that we obtained before, going to zero at long times due to the Orthogonality Catastrophe. In the theory of open systems, one typically uses a related function, the so called Loschmidt echo $L(t) = |\nu_{\beta}(t)|^2$, which gives a measure of the environmental response to the perturbation induced by the system [12, 13, 23] and which, as shown in Ref. [17], is linked with non-Markovianity of the open system dynamics. The amount of non-Markovianity of a dynamical map can be evaluated in different manners [14–16], which are, however, essentially equivalent for a purely dephasing quantum channel [17, 24]. By adopting the definition in terms of information flow given in [14], one finds

$$\mathcal{N} = \sum_{n} |\sqrt{L}(t_{\mathrm{MAX},n})| - |\sqrt{L}(t_{\mathrm{MIN},n})|\,, \tag{21}$$

where the sum is performed over all maxima and minima of the Loschmidt echo. Using our previous results for the amplitude $\nu_{\beta}(t)$, we can then obtain the non-Markovianity of the dynamics of a two-level system in a trapped Fermi gas. The results are shown in Fig. 4**B**, where we see that $\mathcal{N}$ depends on the temperature and on the critical parameter α. In particular, it goes to zero both for large temperatures (due to the fact that thermal fluctuations suppress oscillations in the persistence amplitude) and for $\alpha > 1$.

In the latter case, excitations are generated at every energy scale in the fermion gas, as witnessed by the fact that the spectrum becomes structure-less. This implies that the gas becomes more and more stiff (in the sense that it is not able

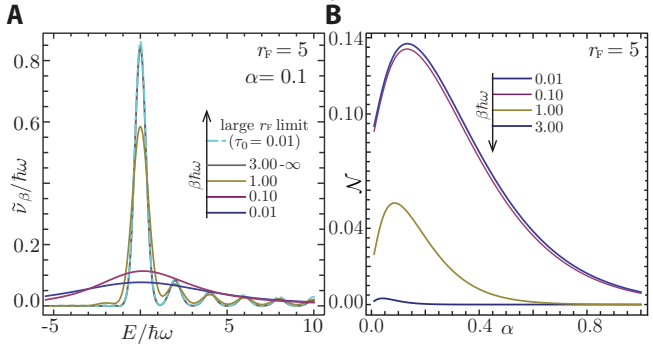

FIG. 4. (color online): **(A)** Absorption spectrum $\nu'_{\beta}(E)$, calculated numerically from eq. (18) with $\beta\hbar\omega = 0.1-\infty$, $r_{\mathrm{F}} = 5$, and $\alpha = 0.1$, and analitycal approximation $\nu'_{\infty}(E)$ obtained from eq. (19); **(B)** Non-Markovianity measure as a function of the critical parameter α for various temperatures.

to react on the impurity any more). This explains why $\mathcal{N}$ is zero: the open system does not receive information back, its Loschmidt echo decays monotonously and thus the dynamics is Markovian. As a result, we conclude that a non-Markovian dynamics can be characterized, in our case, by the appearance of specific spectral features in the excitation energy distribution [25].

We conclude with two final remarks. The first one is that the spectral distribution of energy excitations we have obtained above coincides with the so called work distribution function, which is a central quantity in non-equilibrium processes [26]. In the set-up that we have described above, it is simple enough to imagine a 'reverse' protocol, with the fermi gas brought to thermal equilibrium in the presence of the impurity (i.e. with the two-level atom in the excited state) which is then switched off. The comparison of the work distribution functions in the direct and reverse protocols would lead to a direct experimental test of the Crooks relation in the quantum regime [27]. Finally, we remark on the experimental realization of the model we have described. Many experiments have recently dealt with the effects of impurities in trapped Fermi gas [28], and state-dependent scattering lengths have been discussed [29]. This would lead to a direct test of our theory. Another viable candidate could be a gas of hard-core bosons in one-dimension, where the Loschmidt echo is equivalent to that of the corresponding Fermi gas [30] and in which impurities have recently been experimentally generated [31].

[1] P. W. Anderson, Phys. Rev. Lett. **18**, 1049 (1967).
[2] G.D. Mahan, Phys. Rev. **163**, 612 (1967).
[3] P. Nozieres and C.T. De Dominicis, Phys.Rev. **178**, 1097 (1969); R. Roulet, J. Gavoret and P. Nozieres, Phys.Rev. **178**,

1072 (1969); P. Nozieres, J. Gavoret and R. Roulet, Phys.Rev. **178**, 1084 (1969).
[4] A. Sindona *et al*., Surf. Sci., **601**, 2805 (2007); A. Sindona, M. Pisarra, P. Riccardi, G. Falcone, Nanosci. Nanotechnol. Lett. **3**, 835 (2011).
[5] M. Heyl and S. Kehrein, Phys. Rev. B **85**, 155413 (2012).
[6] N. Ubbelohde *et al.*, Sci. Rep. **2**:374, 1 (2012).
[7] M. Hentschel and F. Guinea, Phys. Rev. B **76**, 115407 (2007).
[8] A. Sindona, R.A. Baragiola, G. Falcone, A. Oliva, P. Riccardi, Phys. Rev. A **71**, 052903 (2005)
[9] D. P. Clougherty and Y. Zhang, Phys. Rev. Lett **109**, 120401 (2012).
[10] J. Goold, T. Fogarty, N. Lo Gullo, M. Paternostro, and T. Busch, Phys. Rev. A **84**, 063632 (2011).
[11] M. Knap *et al*., arXiv:1206.4962 (2012).
[12] A. Peres, Phys. Rev. A **30**, 1610 (1984); T. Gorin *et al*., Phys. Rep. **435**, 33 (2006).
[13] F. M. Cucchietti, *et al*., Phys. Rev. Lett. **91**, 210403 (2003).
[14] H. P. Breuer, E.-M. Laine, and J. Piilo, Phys. Rev. Lett. **103**, 210401 (2009).
[15] A. Rivas, S. F. Huelga, and M. B. Plenio, Phys. Rev. Lett. **105**, 050403 (2010).
[16] X. M. Lu, X. Wang, and C. P. Sun, Phys. Rev. A **82**, 042103 (2010).
[17] P. Haikka et al., Phys. Rev. A **85**, 060101(R) (2012).
[18] T. J. G. Apollaro *et al*., Phys. Rev. A **83**, 032103 (2011); S. Lorenzo, F. Plastina, and M. Paternostro, arXiv:1205.4535 (2012).
[19] P. Haikka *et al*. Phys. Rev. A **84**, 031602(R) (2012).
[20] B-H. Lieu et al., Nat. Phys. **7**, 931 (2011).
[21] A. Chiuri *et al*., arXiv:1208.1630 (2012).
[22] See the Supplementary Material for details of the derivation.
[23] P. Zanardi and N. Paunkovíc, Phys. Rev. E. **74**, 031123 (2006).
[24] H.-S. Zeng *et al*., Phys. Rev. A **84**, 032118 (2011).
[25] Similar conclusions have been reported in W.-M. Zhang *et al*., Phys. Rev. Lett. **109**, 170402 (2012).
[26] M. Campisi, P. Hänggi, and P. Talkner, Rev. Mod. Phys. **83**, 771 (2011).
[27] M. Heyl and S. Kehrein, Phys. Rev. Lett. **108**, 190601 (2012).
[28] A. Schirotzek *et al*., Phys. Rev. Lett. **102**, 230402 (2009); C. Kohstall *et al*., Nature **485**, 615 (2012); M. Koschorreck *et al*., Nature **485**, 619 (2012).
[29] K. M. Daily, D. Rakshit, and D. Blume, Phys. Rev. Lett. **109**, 030401 (2012).
[30] K. Lelas, T. Ševa, and H. Buljan, Phys. Rev. A **84**, 063601 (2011); K. Lelas, T. Ševa, H. Buljan and J. Goold, Phys. Rev. A **86**, 033620 (2012).
[31] S. Palzer, C. Zipkes, C. Sias, and M. Köhl, Phys. Rev. Lett. **103**, 150601 (2009); J. Catani *et al*., Phys. Rev. A **85**, 023623 (2012).

Supplementary Material

APPENDIX A: IMPURITY POTENTIAL

The impurity, δ-like potential $V(x)$ employed in this work is localized at the minimum of the harmonic well, thus, it induces excitations that connect only unperturbed one-fermion states labelled by even numbers $n = 2r$. The diagonal matrix elements of $V(x)$, shown in Fig. 5**A**, entirely determine the one-vertex graph of Eq. (6) of the main text, representing first order corrections to the single-particle energies $\varepsilon_n = \hbar\omega\,(n + 1/2)$. In addition, both diagonal and off-diagonal matrix elements of $V(x)$, the latter shown in Fig. 5**B**, appear as absolute squares in the two-vertex graph $\Lambda_2^\beta(t)$.

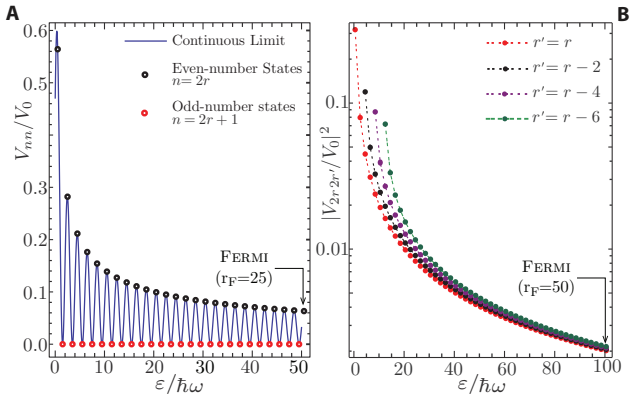

FIG. 5. (color online): (**A**): First order energy shifts for the occupied fermion levels ε_n of the trap. The continuous limit representation of V_{nn} is obtained by letting n take any real value between 0 and $2r_{\rm F}$, which corresponds to the $\omega \to 0$-limit. (**B**): Second order couplings between even one-fermion states that enter the two-vertex graph of Eq (7).

APPENDIX B: NUMERICAL COMPUTATIONS

The quantities involved in our model for the vacuum persistence amplitude $\nu_\beta(t)$ are:

- the energy of the fermion gas in the harmonic trap (E_0^β), together with the first and second order shifts due to the impurity potential (e.g., E_1^β and E_2^β, reported in Eqs. (8) and (12) of the main text);
- the gaussian damping coefficient g_β, entering the sub-diagram $\Lambda_{2\rm G}^\beta$, given as Eq.(14) and (13) in the main text, respectively;
- the Fermi edge loop $\Lambda_{2\rm P}^\beta$ reported in Eq. (15).

These contributions contain summations running over all one-fermion eigenstates of the trap that we truncated by using a high energy cut-off $\varepsilon_{\rm CUT} \gg \varepsilon_{\rm F}$. To fix $\varepsilon_{\rm CUT} = \hbar\omega\,(2r_{\rm CUT} + 1/2)$, we performed convergency tests by changing $r_{\rm CUT}$ in order to have a maximum instability error below 0.1%. We observed that accurate estimations of E_2^β and g_β require values of $r_{\rm CUT}$ in the range of 10^3 to 5×10^3 for $r_{\rm F}$ below ~ 100 and $\beta\hbar\omega$ larger than ~ 0.1. In particular, the plots of Fig. 1**C** and Fig. 2**A** were generated with a energy cut-off of $25 - 500\ \varepsilon_{\rm F}$. As for E_0^β, E_1^β, and $\Lambda_{2\rm P}^\beta$, we found out a cut-off of $\sim 10\ \varepsilon_{\rm F}$ to be sufficient in the investigated range of fermion numbers and temperatures. Accordingly, in fig. 1**A**, fig. 1**B**, and fig. 2**C**, we included up to 10^3 one-fermion states.

APPENDIX C: ANALYTICAL APPROXIMATION FOR THE TWO-VERTEX GRAPH

The expression of the free fermion propagator, reported in Eq. (4) of the main text, and the power series expansion

$$f_r = \begin{cases} \sum_{m=0}^{\infty}(-1)^m e^{2m\beta\hbar\omega r} & r < 0 \\ 1/2 & r = 0 \\ \sum_{m=0}^{\infty}(-1)^m e^{-2(m+1)\beta\hbar\omega r} & r > 0 \end{cases} \tag{22}$$

of the statistical Fermi factors $f_{r-r_{\rm F}}$, allow us to manipulate the connected diagrams entering $\nu_\beta(t)$, and find analytical expressions for $\Lambda_{2\rm G}^\beta(t)$ and $\Lambda_{2\rm P}^\beta(t)$.

In particular, we may rewrite the gaussian damping coefficient introduced in Eq. (14) of the main text as

$$g_\beta = \frac{{}_2\Gamma_1\,(r_{\rm F})^2}{4} + \sum_{m=1}^{\infty}(-1)^m\, m\, g_m^\beta\,(r_{\rm F})\,, \tag{23}$$

in which the finite temperature summand

$$\begin{aligned} g_m^\beta\,(r_{\rm F}) = {}& {}_2\Gamma_1\,(r_{\rm F})^2\ {}_3\tilde{F}_2(r_{\rm F}, e^{2m\beta\omega\hbar}) \\ & - {}_2\Gamma_1\,(r_{\rm F}+1)^2\, e^{-2\beta m\omega\hbar}\, {}_3\tilde{F}_2(r_{\rm F}+1, e^{-2m\beta\omega\hbar}) \\ & - 2\,K\left(e^{2m\beta\omega\hbar}\right)\, e^{-2\beta m\omega\hbar r_{\rm F}} \end{aligned} \tag{24}$$

depends on the generalized hypergeometric function

$${}_3\tilde{F}_2(r_{\rm F}, z) = {}_3F_2\left(1, r_{\rm F}+1/2, r_{\rm F}+1/2 | r_{\rm F}+1, r_{\rm F}+1 | z\right), \tag{25}$$

and the complete elliptic integral of the first kind K.

We consider a many fermion environment ($r_{\rm F} \gg 1$), approximating g_m^β with the large-$r_{\rm F}$ expansion

$$g_m^\beta\,(r_{\rm F}) \approx \frac{1}{4r_{\rm F}} - \frac{2}{r_{\rm F}}\sum_{m=1}^{\infty}\frac{(-1)^m m}{e^{2m\beta} - 1} \tag{26}$$

that works extremely well for $r_{\rm F} \gtrsim 10$ and $\beta \gtrsim 0.5$. The asymptotic form of g_β leads to the result reported as Eq. (16) in the main text.

As for the Fermi-edge component $\Lambda_{2\rm P}^\beta$, we work on the auxiliary functions introduced in Eq (5) of the main text and use

the power series expansion reported in Eq.(22) above, to write

$$\lambda_{\pm}^{\beta}(t) = \sum_{m=0}^{\infty}(-1)^m \sum_{r=0}^{r_{\rm F}-1} l_{r\,m}^{\pm}\, e^{\pm 2\omega r i t} + {}_2\Gamma_1\left(r_{\rm F}\right)\frac{e^{\pm 2 i r_{\rm F}\omega t}}{2} + \sum_{m=0}^{\infty}(-1)^m \sum_{r=r_{\rm F}+1}^{\infty} l_{r-m-1}^{\pm}\, e^{\pm 2\omega r i t}, \tag{27}$$

with $l_{r\,m}^{+} = {}_2\Gamma_1\left(r\right)\, e^{2m\beta\hbar\omega(r-r_{\rm F})}$, and $l_{r\,m}^{-} = l_{r\,m+1}^{+}$. Next, we consider the summations

$$\sum_{r=0}^{r_{\rm F}-1} {}_2\Gamma_1\left(r\right)\, z^r = \frac{\sqrt{\pi}}{\sqrt{1-z}} - z^{r_{\rm F}}\, {}_2\tilde{F}_1(r_{\rm F}, z), \tag{28}$$

and

$$\sum_{r=r_{\rm F}+1}^{\infty} {}_2\Gamma_1\left(r\right)\, z^r = z^{r_{\rm F}+1}\, {}_2\tilde{F}_1(r_{\rm F}+1, z), \tag{29}$$

holding for any $z \neq 1$, where ${}_2\tilde{F}_1$ is the regularized ${}_2F_1$-Hypergeometric function

$${}_2\tilde{F}_1(r_{\rm F}, z) = {}_2\Gamma_1\left(r_{\rm F}\right)\, {}_2F_1\left(1, r_{\rm F}+1/2, r_{\rm F}+1; z\right), \tag{30}$$

having the asymptotic behavior

$${}_2\tilde{F}_1(r_{\rm F} \gg 1, z) = \frac{r_{\rm F}^{-1/2}}{1-z} + o\left(r_{\rm F}^{-3/2}\right). \tag{31}$$

With the representation (27), we need to add an imaginary time regularization to the t''-integral in the two-loop term, e.g., we have to shift the t'' integration domain by $i\tau_0$ to prevent ${}_2\tilde{F}_1(r_{\rm F}, e^{\pm 2\omega r i t''})$ and ${}_2\tilde{F}_1(r_{\rm F}+1, e^{\pm 2\omega r i t''})$ from being singular. We, then, insert eq. (27) in the expression for $\Lambda_2^{\beta}(t)$, compute the r-summations, and use the large $r_{\rm F}$ expansion (31). Finally, we perform the t' and t''-integrals, excluding terms proportional to t and t^2. What is left is a combination of logarithmic and polylogarithmic functions, dominated by the Fermi-edge term reported in the Eq. (17) of the main text. Indeed, as shown in Fig. 6 the zero temperature form

$$\Lambda_{2\rm P}^{\infty}(t) \approx \ln\left(\frac{e^{2\tau_0\omega}-1}{e^{2\omega(\tau_0+it)}-1}\right)^{\alpha} \tag{32}$$

obtained from this procedure is in excellent agreement with the numerical calculations reported in Fig. 2**B** for $r_{\rm F} \sim 100$ and $\beta\hbar\omega$ larger than ~ 1. The correctness of such an approximation is also attested by the comparison of Fig 5**A**.

APPENDIX D: DECOHERENCE FACTOR AND ABSORPTION SPECTRUM

We performed numerical calculations of the decoherence factor $|\nu_\beta(t)|$, and the environment absorption spectrum $\tilde{\nu}_\beta(E)$, by selecting different fermion numbers ($r_{\rm F} = 5 - 100$), coupling parameters ($\alpha = 0 - 1.1$), and thermal energies ($\beta\hbar\omega = 0.001 - 10$). In the main text, we have presented an application to a Fermi gas of 200 particles (in Fig. **3**) where the Fermi-edge behavior, superimposed on a gaussian damping trend, appears as a sequence of spikes in $|\nu_\beta(t)|$ and an asymmetric peak structure in $\tilde{\nu}_\beta(E)$. Such features become more and more marked with decreasing temperature, which reduces the effect of the gaussian coefficient g_β (see Fig. 2**A**), whereas they disappear for $\alpha > 1$. Similar considerations hold for environments containing low numbers of fermions (see Fig. 7) in which shake-up effects are even more visible because of the decreasing of g_β with decreasing $\varepsilon_{\rm F}$. On the other hand, the approximation given by Eq. (18) in the main text works extremely well with environments containing

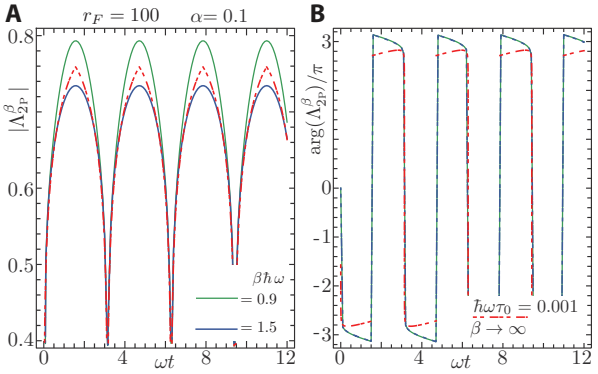

FIG. 6. (color online) Absolute value (**A**) and phase (**B**) of the Fermi edge diagram $\Lambda_{2\rm P}^{\beta}$, for $\alpha = 0.1$ and $2r_{\rm F} = 100$. Numerical computations from Eq. (15), for $\beta\hbar\omega = 0.9, 1.5$ are compared with the $\beta \to \infty$ approximation obtained from Eq. (32).

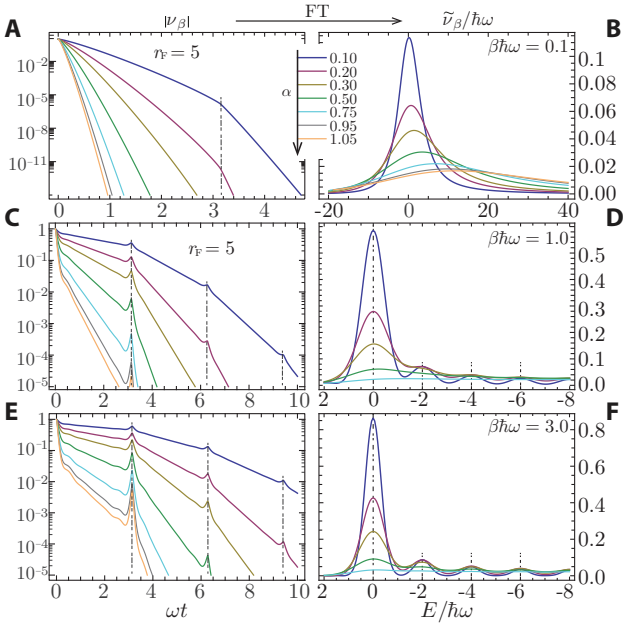

FIG. 7. (color online): Absolute value of the decoherence factor $|\nu_\beta(t)|$ (left panels, **A**,**C**,**E**) and absorption spectrum $\nu'_\beta(E)$ (right panels, **B**,**D**,**F**), calculated from Eq. (18) of the main text by numerically computing the sub-diagrams of Eqs. (13) and (15), for $\beta\hbar\omega = 0.1 - 10$, $r_{\rm F} = 5$, and $\alpha = 0.1 - 1.05$.

large fermion numbers. Nevertheless, we noticed that values of $r_{\rm F}$ larger than ~ 10 are sufficiently well reproduced by the analytical model, at any temperatures.

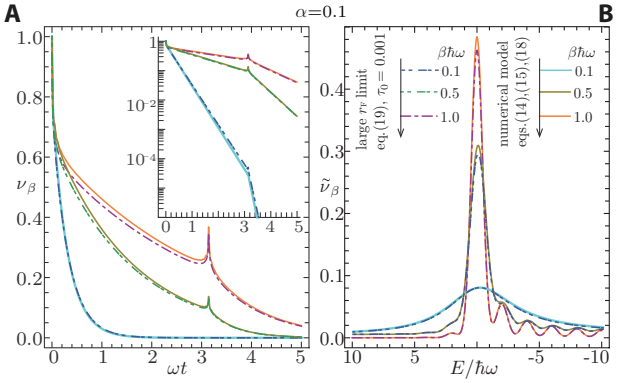

FIG. 8. (color online): Absolute value of the decoherence factor $|\nu_\beta(t)|$ (**A**) and absorption spectrum $\nu'_\beta(E)$ (**B**), calculated from Eq. (18) of the main text by numerically computing the sub-diagrams of Eqs. (13) and (15), by including 2000 m-products, for $\beta\hbar\omega = 0.1 - 1$, $r_{\rm F} = 50$, and $\alpha = 0.4$.